Available online www.ejaet.com

European Journal of Advances in Engineering and Technology, 2020, 7(12):9-20

Research Article ISSN: 2394 - 658X

Novel Predictive Torque Control Strategies for Two-Level Inverter Fed Induction Motor Drives

Wiem ZOUARI, Imen NOUIRA EL BADSI and Bassem EL BADSI*

Laboratory of Renewable Energies and Electric VehiclesUniversity of Sfax, P.O. Box 1173, 3038 Sfax, Tunisia
**Corresponding Author – bassemelbedsi@yahoo.fr*

ABSTRACT

Conventional predictive torque control (C-PTC) uses all voltage vectors generated by the two-level (B6) inverter for prediction, optimization, and actuation. In addition, C-PTC method leads to high switching power losses if during two consecutive sampling periods two opposite voltage vectors are applied as optimal vectors. To overcome these issues, this paper develops two improved PTC methods based on the phase-clamping (PC) technique. The proposed PC-PTC methods are founded on the basis of modulating two inverter legs instead of the three ones by clamping, during each 60° sub-cycle, one stator phase to the positive or negative terminals of the dc-bus voltage. The improvements gained by the proposed PC-PTC methods, in terms of reduction of switching frequency, stator current THD, and torque ripple, are proved through simulation and experimental results.

Key words: Predictive torque control, Induction motor, Phase-clamping technique, Switching frequency, Total harmonic distortion

---

INTRODUCTION

As an effective alternative to the direct torque control (DTC) strategy, predictive torque control (PTC) strategy has been adopted in several applications thanks to its simple control scheme. However, his major drawbacks are the high current harmonic distortion, switching power losses, and torque ripple. Moreover, many PTC schemes present simple bloc diagrams, except that the predefined switching table of DTC is replaced by an online optimization algorithm. The main concept of all PTC schemes is based on the prediction of the future system behaviours, namely: stator current vector, stator flux vector, and electromagnetic torque, in order to identify the optimal voltage vector that reduces the flux and torque ripples [1-4].

In the C-PTC, the prediction, optimization and actuation steps involve all the voltage vectors generated by the two-level (B6) inverter, which increase the calculation burden in the control system. Furthermore, if two opposite voltage vectors are applied as optimal vectors, during two consecutive sampling periods, the states of all power switches commutate, which increases the switching power losses in the B6 inverter. To solve this issue, an approach based on adding a switching transition term in the cost function has been adopted in [5-7]. Nonetheless, such a solution requires the selection of a new weighting factor and further increases the computational burden, which limits the reduction of the sampling period of the control system. In [3], the number of prediction vectors is reduced and the switching frequency is mitigated without the requirement of the switching-transition term in the cost function. However, the problem of applying two opposite voltage vectors during two consecutive sampling periods has not been solved.

In addition, the reduction of the harmonic distortion in the stator phase currents of the induction motor (IM) is a crucial guide line for satisfactory operation in variable speed drives. Unfortunately, current harmonic distortion can't be considered in the design of the cost function. In fact, the optimization step investigates, in each sampling period, only the errors of the controlled variables (torque and flux), regardless to the harmonic distortion level in the IM stator phase currents.

To improve the steady-state performance, various methods based on the application of two voltage vectors during one control period have been developed [10-17]. To achieve satisfactory performance, the two-vector-based PTC methods require high sampling frequency, since that the corresponding duty cycles should be calculated during each control period.

In order to preserve the simplicity of the C-PTC bloc diagram and to avoid the need to increase of the sampling frequency, this paper treats a comparative study of three simplified PTC methods for B6inverter fed IM drives. In addition to C-PTC, two novel PTC methods are developed considering the well known phase-clamping (PC) techniques. In fact, these latter are firstly introduced in the design of the space-vector modulation (SVM) techniques, which are the most popular real-time methods enabling the control of the voltage source inverter with the lowest harmonic distortion of the output voltages and currents [11-13]. Further improvements in terms of reducing the switching frequency and torque ripple can be gained by using the PC-SVM methods which allow, during a predetermined sub-cycle of the stator variables period, the clamping of one stator phase connected to the high or low levels of the dc-bus voltage. Recently, it has been proved that integrating the PC technique in the DTC strategy reduces the current harmonic distortion, switching frequency, and torque ripple, especially at low speed operation [14-15]. Within this approach, two phase-clamping PTC (PC-PTC) methods are proposed on the basis of the clamping of each stator phase during two 60° sub-cycles at every stator variables period [16].

The effectiveness of the three PTC methods are evaluated at a first step through simulation works considering various performance criteria, namely: (i) the average switching frequency, (ii) the average total harmonic distortion of the three stator phase currents, (iii) the stator flux ripple, and (iv) the electromagnetic torque ripple. In a second step, an experimental setup of a B6 inverter fed IM drive has been done in order to verify and prove the results obtained by simulation. The comparative study shows that the proposed PC-PTC methods, compared to C-PTC, exhibit much better performance in terms of reduction of switching frequency, stator current THD, and torque ripple, especially at low speed levels.

CONVENTIONAL PTC METHOD

The block diagram of the conventional PTC (C-PTC) of the B6 inverter fed IM drive, shown in Fig. 1, involves: (i) the estimation of the stator flux, (ii) the prediction of the stator and rotor fluxes, stator current, and electromagnetic torque, (iii) the optimization of a cost function, and (iv) an external proportional-integral (PI) speed controller.

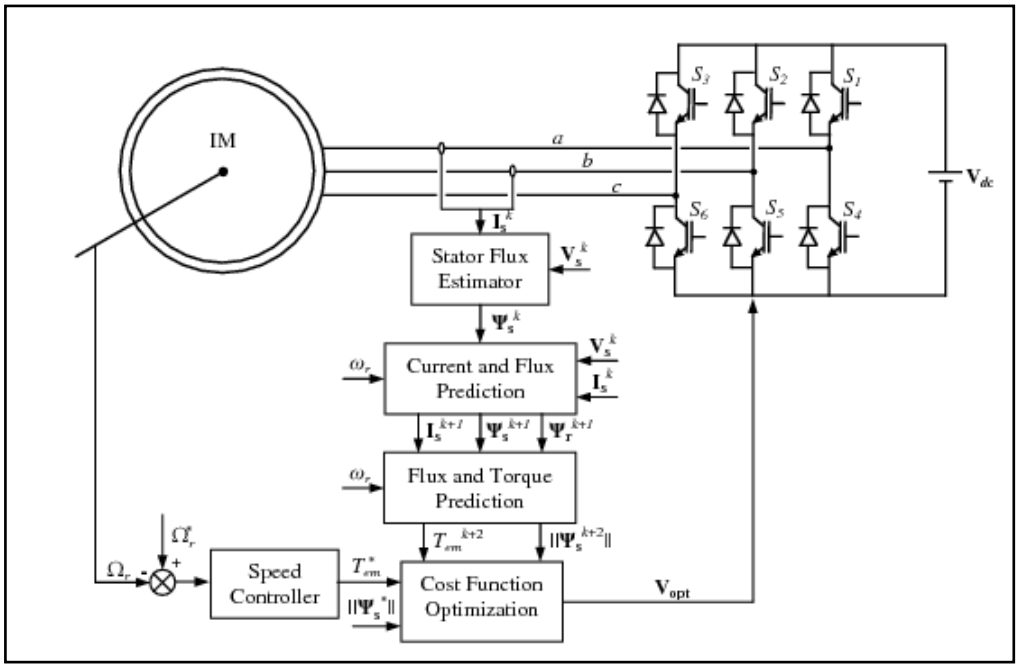

Fig. 1 Block diagram of C-PTC method for B6 inverter fed IM drive

Concerning the B6 inverter, eight possible combinations of ($\mathbf{S}_1$, $\mathbf{S}_2$, $\mathbf{S}_3$) define, in the $\alpha\beta$-plane, eight voltage vectors $\mathbf{V}_i$. The prediction and optimization steps involve all of these eight voltage vectors. The cost function represents a combination of the objective functions, to establish the optimum voltage vector $\mathbf{V}_{opt}$ to be applied in the next sampling period.

Dynamic Model of IM

In the stationary $\alpha\beta$-frame, the stator and rotor voltage vectors are given as follows:

$$V_s = \frac{d\psi s}{dt} + r_s I_s \qquad (1)$$

$$0 = \frac{d\psi r}{dt} + r_r I_r - \omega_r J \psi_r$$

where $\mathbf{I}_s$, ψ_s, and ψ_r denote the stator current, the stator flux, and the rotor flux vectors, respectively; r_s, r_r, and ω_r are the stator resistance, the rotor resistance, and the rotor angular frequency, respectively; J is an orthogonal matrix defined by:

$$\left(J = \begin{matrix} 0 \\ 1 \end{matrix} \right) \begin{matrix} -1 \\ 0 \end{matrix} \tag{2}$$

The stator and rotor flux vectors can be defined as:

$$\begin{aligned} \psi_s &= l_s I_s + M I_r \\ \psi_r &= M I_s + l_r I_r \end{aligned} \tag{3}$$

where l_s, l_r, and M are the stator self, the rotor self, and the mutual inductances, respectively.

The electromagnetic torque T_{em} can be expressed as follows where N_p is the pole pairs and $\lambda = 1/(l_s l_r - M^2)$:

$$T_{em} = \frac{3}{2} N_p \lambda M (\psi_r \times \psi_s) \tag{4}$$

Flux Estimation

According to (1) and (3), the estimation of $\boldsymbol{\psi}_s$ and $\boldsymbol{\psi}_r$ can be derived as:

$$\begin{aligned} \hat{\psi}_s^k &= \int (V_s^k - r_s I_s^k) dt \\ \hat{\psi}_r^k &= \frac{\hat{l}_r}{M} \psi_s^k - \frac{1}{\lambda M} I_s^k \end{aligned} \tag{5}$$

Flux and Torque Prediction

To predict flux and torque, the *Heun*'s method is adopted as in [17]-[19]. Hence, the predictor corrector of the stator current and flux vectors are expressed as:

$$\begin{bmatrix} I_{sp}^{k+1} \\ \psi_{sp}^{k+1} \end{bmatrix} = \begin{bmatrix} I_s^k \\ \psi_s^k \end{bmatrix} + \left(\begin{bmatrix} T_s & A_{11} \\ & A_{21} \end{bmatrix} \begin{bmatrix} A_{12} \\ 0 \end{bmatrix} \begin{bmatrix} I_s^k \\ \psi_s^k \end{bmatrix} + \begin{bmatrix} \lambda l_r V_s^k \\ V_s^k \end{bmatrix} \right) \tag{6}$$

Where:

$A_{11} = -\lambda(r_s l_r + r_r l_s) + j\omega_r$

$A_{12} = \lambda(r_r - j l_r \omega_r)$

$A_{21} = -r_s$

Therefore, the predicted current and flux vectors can be derived as [17]-[19]:

$$\begin{bmatrix} I_s^{k+1} \\ \psi_s^{k+1} \end{bmatrix} = \begin{bmatrix} I_{sp}^{k+1} \\ \psi_{sp}^{k+1} \end{bmatrix} + \frac{T_s}{2} \left(\begin{bmatrix} A_{11} & A_{12} \\ A_{21} & 0 \end{bmatrix} \begin{bmatrix} I_{sp}^{k+1} - I_s^k \\ \psi_{sp}^{k+1} - \psi_s^k \end{bmatrix} \right) \tag{7}$$

Then, the rotor flux and the electromagnetic torque at the $(k + 1)^{th}$ sampling period can be predicted as follows:

$$\psi_r^{k+1} = \frac{l_r}{M} \psi_s^{k+1} - \frac{1}{\lambda M} I_s^{k+1} \tag{8}$$

$$T_{em}^{K+1} = \frac{3}{2} N_p \lambda M (\psi_r^{k+1} \times \psi_s^{k+1}) \tag{9}$$

Cost Function Optimization

The cost function g is based on the square values of the electromagnetic torque and stator flux errors with the weighting flux factor k_g. It is defined as:

$$g = \frac{(T_{em}^* - T_{em}^{K+2})^2}{T_{emR}^2} + k_g \frac{(\,|\|\psi_s^*\| - \|\psi_s^{K+2}\|\,)^2}{\|\psi_{sR}\|^2} \tag{10}$$

where T_{em}^* is the reference torque produced by the external PI-speed controller, $\| \psi_s^* \|$ is the amplitude of the reference stator flux, T_{emR} and $\|\psi_{sR}\|$ are, respectively, the rated torque and flux. The weighting flux factor k_g can be defined by various approaches based on analytical or empirical methods [20]-[22].

The optimization step is based on the minimization, at each sampling period T_s, of the predefined cost function. The optimal voltage vector $\mathbf{V}_{opt}$ is the one which minimizes the cost function, and it is selected to be applied at the $(k+1)^{th}$ sampling period. In order to compensate the one-step delay in real-time implementation, the variables at $(k+2)^{th}$ sampling period should be predicted.

PROPOSED PHASE-CLAMPING-BASED PTC METHODS

In the C-PTC strategy, the prediction, optimization and actuation steps involve all voltage vectors generated by the B6 inverter, which increase the calculation burden in the control system. In addition, if during two successive sampling periods two opposite voltage vectors are applied as optimal vectors, the states of the six power switches commutate, which rises the switching power losses in the B6 inverter. Furthermore, reducing the harmonic distortion of the stator phase voltages and currents represents a fundamental criterion to ensure efficient operation in variable speed drives. However, the optimization step examines just the errors of the controlled variables (torque and flux) regardless to the harmonic distortion level in the IM phase voltages and currents.

It is commonly known that the space-vector modulation (SVM) techniques offer the lowest harmonic distortion of the IM phase currents as well as the mitigation of the switching power losses in the inverter. The SVM methods select the adequate space voltage vectors and their appropriate durations to approximate a revolving reference voltage vector. Further improvement in terms of reduction of switching losses can be gained by using the phase-clamping SVM (PC-SVM) method, which allows the maintain of one stator phase linked, during a determined sub-cycle of the stator variables period T_s, to the high or low levels of the dc-bus voltage $\mathbf{V}_{dc}$.

In this paper, two phase-clamping-based PTC (PC-PTC) methods are developed. The bloc diagram of the proposed PC-PTC are almost similar to that of the C-PTC [23]. Nonetheless, in the PC-PTC and during every one-sixth of T_s, only four vectors $\mathbf{V}_i$ (one zero and three active ones) are evaluated for the prediction, optimization, and actuation. Indeed, as in the PC-SVM techniques, both proposed PC-PTC methods (PC-PTC1 and PC-PTC2) allow the clamping, during each 60° sub-cycle, of one stator phase to the positive or negative terminals of the dc-bus voltage $\mathbf{V}_{dc}$. The major difference between them is the approach adopted in the selection of the clamped phase.

PC-PTC1 Method

In the PC-PTC1 method, the revolving reference vector is the stator flux $\boldsymbol{\psi}_s$ with an angular position defined as:

$$\theta_{\psi s} = \arctan\left(\frac{\psi\beta s}{\psi\alpha s}\right) \tag{11}$$

As illustrated in Fig.2, the αβ-plane is divided into six equal sectors i (I to IV), which define the position of the stator flux vector $\boldsymbol{\psi}_s$ and can be numerically derived as:

$$\text{Sector i: } (2i-3)\frac{\pi}{6} \leq \theta_{\psi s} < (2i-1)\frac{\pi}{6} \tag{12}$$

The following analysis considers the case when $\boldsymbol{\psi}_s$ is located in sector I. Referring to equation (1) and by neglecting the voltage drop $r_s.I_s$, the corresponding voltage vector $\mathbf{V}_s$ is 90°-shifted with respect to $\boldsymbol{\psi}_s$. As shown in Fig. 2, $\mathbf{V}_s$ can be located between the two active voltage vectors $\mathbf{V}_2$ and $\mathbf{V}_3$ for the case of an anti-clockwise rotation, or between $\mathbf{V}_5$ and $\mathbf{V}_6$ for the case of a clockwise rotation.

As a result, the approximation of $\mathbf{V}_s$ could be accomplished by the application of vectors $\mathbf{V}_2$, $\mathbf{V}_3$, and one null voltage vector $\mathbf{V}_0^1$ or $\mathbf{V}_0^2$, according to the PC-SVM methods. Thus, the prediction and optimization steps can be achieved, during sector I, considering two possible sets of $\mathbf{V}_i$, such as:

1) $\mathbf{V}_2$, $\mathbf{V}_3$, and $\mathbf{V}_0^1$: to clamp the stator c-phase to the low-level of the dc-bus voltage (c^-). With these vectors, it is possible to add vector $\mathbf{V}_1$, which also allows the clamping of c^-.

2) $\mathbf{V}_2$, $\mathbf{V}_3$, and $\mathbf{V}_0^2$: to clamp the stator b-phase to the high-level of the dc-bus voltage (b^+). With these vectors, it is possible to add vector $\mathbf{V}_4$, which also allows the clamping of b^+.

Therefore, one of the stator phases (c^- or b^+) can be clamped during sector I. In this paper, the first set of vectors ($\mathbf{V}_1$, $\mathbf{V}_2$, $\mathbf{V}_3$ and $\mathbf{V}_0^1$), is adopted in the PC-PTC1 strategy during sector I. The same approach can be applied for the remaining sectors, which leads to the clamping of each stator phase during two 60° sub-cycles. Fig. 2 shows the clamped stator phases, in blue colour for the case of an anti-clockwise rotation and in green colour for the case of clockwise rotation.

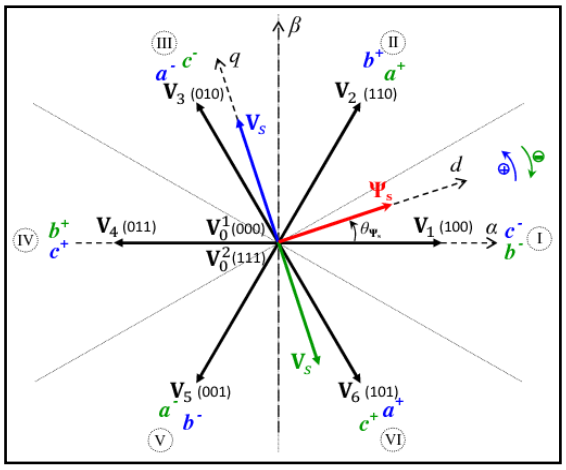

Fig. 2 Stator voltage vectors V_i(S1 S2 S3) and the six sectors i adopted in the PC-PTC1 method

Table-1 and Table-2 summarize the evaluated voltage vectors $\mathbf{V}_i$ and the corresponding clamped phase during each sector i for the case of an anti-clockwise and clockwise rotation of $\boldsymbol{\psi}_s$ respectively. For instance, from the analysis of the vectors set adopted in the first sector, it can be noted that, exception the commutations between $\mathbf{V}_1$ and $\mathbf{V}_3$ which generate two switching transitions, all the other possible commutations lead to one switching transition. Moreover, the third inverter leg keeps the same state ($\mathbf{S}_3 = 0$) during sector I. Accordingly, the proposed PC-PTC minimizes the average switching frequency without the need of a switching transition term in the cost function.

Table-1 Evaluated voltage vectors and clamped phases of PC-PTC1 in anti-clockwise rotation of ψ_s

Sectors	Evaluated Voltage Vectors	Clamped Phases
I	$\mathbf{V}_1\ \mathbf{V}_2\ \mathbf{V}_3\ \mathbf{V}_0^1$	c^-
II	$\mathbf{V}_2\ \mathbf{V}_3\ \mathbf{V}_4\ \mathbf{V}_0^2$	b^+
III	$\mathbf{V}_3\ \mathbf{V}_4\ \mathbf{V}_5\ \mathbf{V}_0^1$	a^-
IV	$\mathbf{V}_4\ \mathbf{V}_5\ \mathbf{V}_6\ \mathbf{V}_0^2$	c^+
V	$\mathbf{V}_5\ \mathbf{V}_6\ \mathbf{V}_1\ \mathbf{V}_0^1$	b^-
VI	$\mathbf{V}_6\ \mathbf{V}_1\ \mathbf{V}_2\ \mathbf{V}_0^2$	a^+

Table-2 Evaluated voltage vectors and clamped phases of PC-PTC1 in clockwise rotation of ψ_s

Sectors	Evaluated Voltage Vectors	Clamped Phases
I	$\mathbf{V}_1\ \mathbf{V}_5\ \mathbf{V}_6\ \mathbf{V}_0^1$	b^-
II	$\mathbf{V}_2\ \mathbf{V}_6\ \mathbf{V}_1\ \mathbf{V}_0^2$	a^+
III	$\mathbf{V}_3\ \mathbf{V}_1\ \mathbf{V}_2\ \mathbf{V}_0^1$	c^-
IV	$\mathbf{V}_4\ \mathbf{V}_2\ \mathbf{V}_3\ \mathbf{V}_0^2$	b^+
V	$\mathbf{V}_5\ \mathbf{V}_3\ \mathbf{V}_4\ \mathbf{V}_0^1$	a^-
VI	$\mathbf{V}_6\ \mathbf{V}_4\ \mathbf{V}_5\ \mathbf{V}_0^2$	c^+

PC-PTC2 Method

In the manner of PC-PTC1, the PC-PTC2 method is also based on the clamping of each stator phase during two 60◦-intervals in each cycle. Nonetheless, the difference between the two methods is the approach adopted in the selection of the clamped phase. Indeed, in the PC-PTC2, the revolving reference vector is the stator current vector $\mathbf{I}_s$ instead of the stator flux $\boldsymbol{\psi}_s$ in the case of PC-PTC1. The angular position of $\mathbf{I}_s$ is defined as:

$$\theta_{\mathbf{I}s} = \arctan\left(\frac{i\beta s}{i\alpha s}\right) \tag{13}$$

Fig. 3 shows the normalized waveforms of the stator phase currents (i_{as}, i_{bs}, i_{cs}) in the case of an anti-clockwise rotation of $\mathbf{I}_s$, which corresponds to the succession "$i_{as} \rightarrow i_{bs} \rightarrow i_{cs}$" in the time scale.

Therefore, the adopted sectors and the corresponding clamped phases, during one period T of the stator currents are also shown in Fig. 3. For instance, let us consider the stator a-phase clamped to:

- ⋆ a+ during sector I: corresponds to an angular opening of 60◦ beginning from the positive wave of i_{as}.
- ⋆ a− during sector IV: corresponds to an angular opening of 60◦ beginning from the negative wave of i_{as}.

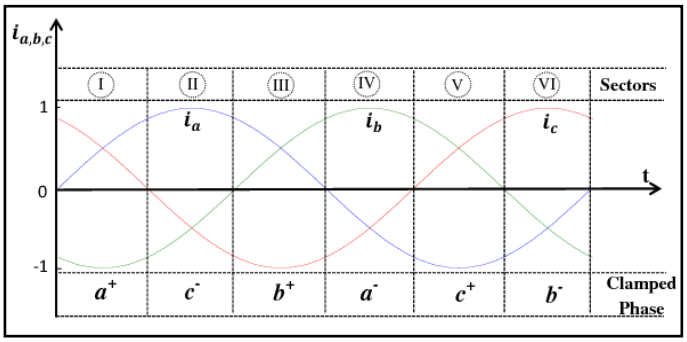

Fig. 3 Normalized waveforms of (i_{as}, i_{bs}, i_{cs}) in the case of an anti-clockwise rotation of I_s.

The same approach is adopted for the stator b- and c-phases, which are clamped twice during one period T_s, as shown in Fig.3. Consequently and as illustrated in Fig. 4, the $\alpha\beta$-plane should be divided into six equal sectors n (I to IV), which define the position of $\mathbf{I}_s$ and can be numerically derived as:

$$\text{Sector } n\text{: } (2n-5)\frac{\pi}{6} \leq \theta_{\mathbf{I}_s} < (2n-3)\frac{\pi}{6} \tag{14}$$

Fig. 4 also shows the clamped stator phases in blue and green colors for the case of an anticlockwise and clockwise rotation of $\mathbf{I}_s$ respectively. For instance, in order to clamp the stator *a*-phase to *a*+ during sector I, four voltage vectors $\mathbf{V_i}$ can be applied, namely: $\mathbf{V_6}$, $\mathbf{V_1}$, $\mathbf{V_2}$, and $\mathbf{V_0}^2$. Table-3 and Table-4 give the evaluated voltage vectors and the corresponding clamped phase during each sector *n* for the case of an anti-clockwise and clockwise rotation of $\mathbf{I}_s$ respectively.

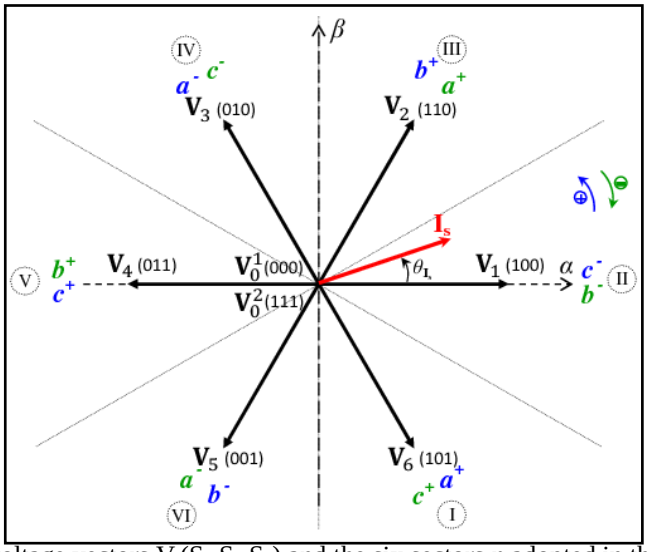

Fig. 4 Stator voltage vectors $V_i(S_1\ S_2\ S_3)$ and the six sectors *n* adopted in the PC-PTC2 method

In order to analyze the case of a clockwise rotation of $\mathbf{I}_s$, one can consider the same waveforms of (i_{as}, i_{bs}, i_{cs}) presented in Fig. 3, while reversing the time axis (i.e. t = T → t = 0 and t = 0 → t = T). Indeed, from sector VI to sector I, the succession of the clamped stator phases is a− → b+ → c− → a+ → b− → c+, as illustrated with green color in Fig. 4.

Table-3 Evaluated voltage vectors and clamped phases of PC-PTC2 in anti-clockwise rotation of ψ_s

Sectors	Evaluated Voltage Vectors	Clamped Phases
I	$\mathbf{V_6}\ \mathbf{V_1}\ \mathbf{V_2}\ \mathbf{V_0}^2$	a^+
II	$\mathbf{V_1}\ \mathbf{V_2}\ \mathbf{V_3}\ \mathbf{V_0}^1$	c^-
III	$\mathbf{V_2}\ \mathbf{V_3}\ \mathbf{V_4}\ \mathbf{V_0}^2$	b^+
IV	$\mathbf{V_3}\ \mathbf{V_4}\ \mathbf{V_5}\ \mathbf{V_0}^1$	a^-
V	$\mathbf{V_4}\ \mathbf{V_5}\ \mathbf{V_6}\ \mathbf{V_0}^2$	c^+
VI	$\mathbf{V_5}\ \mathbf{V_6}\ \mathbf{V_1}\ \mathbf{V_0}^1$	b^-

Table-4 Evaluated voltage vectors and clamped phases of PC-PTC2 in clockwise rotation of ψ_s

Sectors	Evaluated Voltage Vectors	Clamped Phases
I	$\mathbf{V_4}\ \mathbf{V_5}\ \mathbf{V_6}\ \mathbf{V_0}^2$	c^+
II	$\mathbf{V_5}\ \mathbf{V_6}\ \mathbf{V_1}\ \mathbf{V_0}^1$	b^-
III	$\mathbf{V_6}\ \mathbf{V_1}\ \mathbf{V_2}\ \mathbf{V_0}^2$	a^+
IV	$\mathbf{V_1}\ \mathbf{V_2}\ \mathbf{V_3}\ \mathbf{V_0}^1$	c^-
V	$\mathbf{V_2}\ \mathbf{V_3}\ \mathbf{V_4}\ \mathbf{V_0}^2$	b^+
VI	$\mathbf{V_3}\ \mathbf{V_4}\ \mathbf{V_5}\ \mathbf{V_0}^1$	a^-

SIMULATION AND EXPERIMENTAL RESULTS

The performance of the proposed PC-PTC1 and PC-PTC2 methods are analysed and compared to those of the C-PTC method. The ratings and parameters of the induction machine are listed in Tables 5 and 6, respectively. The dc-bus voltage $\mathbf{V}_{dc}$ is kept constant equal to 400V. The amplitude $\| \psi_s^* \|$ of the reference stator flux is equal to 0.947Wb. The sampling period T_s and the weighting factor k_g are kept constant equal to 80µs and 100, respectively.

Table-5 Induction machine ratings

Power	0.37kW	**Efficiency**	77%
Voltage	230V/400V	**Current**	1.7A/1A
Torque	2.56N.m	**Stator Flux (rms)**	0.67Wb
Speed	1380rpm	**Frequency**	50Hz

Table-6 Induction machine parameters

r_s = 24.6Ω	l_s = 0.984H	M = 0.914H	J = 2.5e−3Kg.m2
r_r = 17.9Ω	l_r = 0.984H	N_p = 2	f = 6e−3N.m.s

Simulation Results

Fig. 5 shows the starting responses from standstill to +100rad/s followed by the reverse operation to −40rad/s under a load torque $T_l = \Omega_r/100$ for the C-PTC (subscript "a"), PC-PTC1 (subscript "b"), and PC-PTC2 (subscript "c") methods. From top to bottom, the curves shown in Fig. 5 are rotor speed, control signal S_1, stator phase currents, stator flux amplitude, and electromagnetic and load torques.

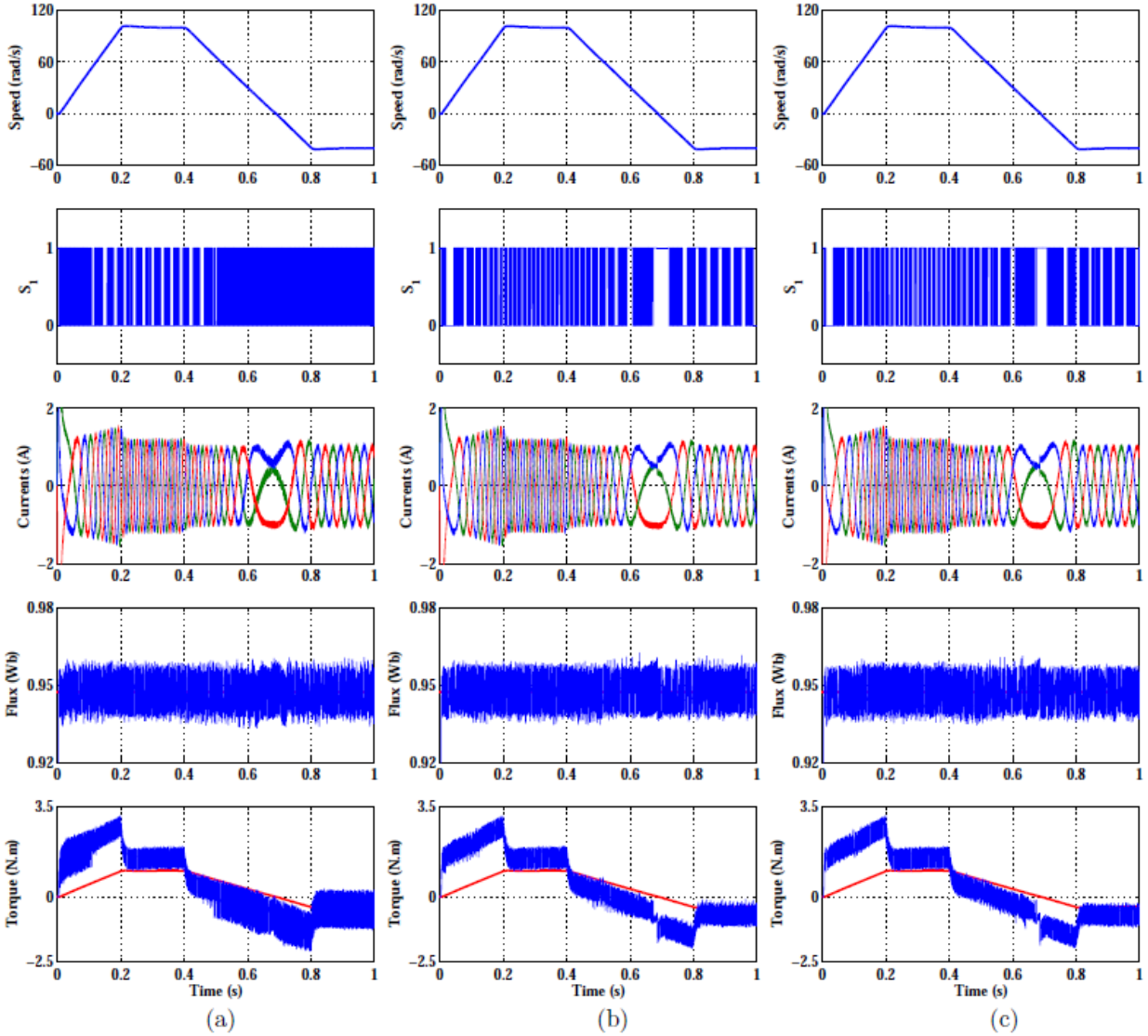

Fig. 5 Simulated transient and steady-state behaviors during a standstill to Ω_r = +100rad/s followed by the reverse operation to
Ω_r = −40rad/s under a load torque $T_l = \Omega_r/100$. Legend (a): C-PTC, (b): PC-PTC1, (c): PC-PTC2.

In order to compare the three PTC methods at both steady-state operating points (Ω_r = +100rad/s at T_l = +1N.m) and (Ω_r = −40rad/s at T_l = −0.4N.m) of Fig. 5, Table-7 gives the values of four performance criteria, such that: (i) the average switching frequency (f_{sw}), (ii) the average total harmonic distortion (THD) of the three stator phase currents, (iii) the stator flux ripple $\Delta||\psi s||$, and (iv) the electromagnetic torque ripple ΔT_{em}.

It is shown that the three PTC methods exhibit high speed responses at transient operation as well as at forward and backward steady-state operations. Furthermore, the stator flux amplitude is almost constant while there are variations in the torque, which confirm that the three PTC methods accomplish decoupled control of flux and torque.

Concerning the waveforms of the electromagnetic torque, it is clearly seen that, compared to the C-PTC strategy, the proposed PC-PTC1 and PC-PTC2 methods mitigate the torque ripple at low speed operation. Indeed, for $|\Omega r| < 60$rad/s (i.e $|\Omega r| < 40\%$ of rated speed), the C-PTC method is penalized by high torque ripple in both forward and backward operations. However, the torque ripple are reduced and almost constant for all operating points under the proposed PC-PTC1 and PC-PTC2 methods.

Furthermore, the transition from the forward to backward rotation, which involves the commutation from table 1 to table-2 for the PC-PTC1 method and the commutation from table 3 to table 4 for the PC-PTC2 method, is performed with high dynamic of the speed responses. It is to be noted that the spikes in the electromagnetic torque at t = 0.7s are the results of the transitions between these tables. However, these torque spikes are lower than the torque ripple exhibited by the C-PTC method at low speeds.

Referring to the control signal S1 and for $|\Omega r| \geq 60$rad/s, one can see that the C-PTC method leads to the clamping of one stator phase during each 120◦ sub-cycle. In fact, if only V10 (respectively, V20) is adopted as zero voltage vector, the stator phases are clamped to a−, b−, and c− (respectively, a+, b+, and c+) during three consecutive 120° sub-cycles. As a result, the phase-clamping technique is self-applied by the C-PTC strategy at high speed operation. Nonetheless, the C-PTC method leads to an excessive switching frequency at low speed operation ($|\Omega r| < 40\%$ of rated speed).

Table-7 Performance comparison at steady-state operating points

Steady-State Operating Point	PTC Method	f_{sw} (kHz)	THD (%)	$\Delta\|\|\psi s\|\|$ (Wb)	ΔT_{em} (N.m)
Ω_r = +100rad/s	C-PTC	3.5	5.2	0.025	0.91
&	PC-PTC1	3.6	5.1	0.025	0.92
T_l = +1N.m	PC-PTC2	3.8	5.4	0.025	0.91
Ω_r = −40rad/	C-PTC	8.23	8	0.024	1.59
&	PC-PTC1	4.98	6.1	0.024	1.07
T_l = -0.4N.m	PC-PTC2	5.63	5.97	0.022	0.95

It can be clearly seen that the proposed PC-PTC1 and PC-PTC2 methods exhibit, at low speed operation, high performances in terms of reduction of switching frequency, stator current THD, and torque ripple. However, the three PTC methods are characterized by similar performances for the case of high speed operation. In order to further evaluate the effectiveness of the proposed PC-PTC methods, the simulation study is focused on the performance criteria f_{sw} and THD, considering different steady-state operating points.

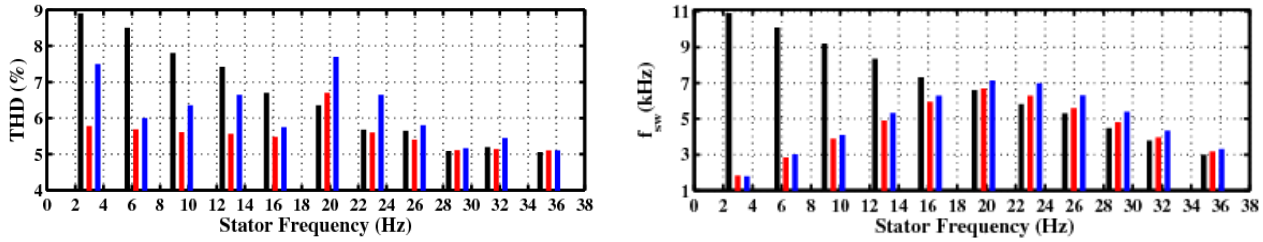

(1) (2)

Fig. 6 Comparison criteria with respect to the stator frequency under a constant load torque T_l = 1N.m.
Legend 1 (a): average switching frequency f_{sw}, (b): average total harmonic distortion THD of the stator phase currents.
Legend 2 (black): C-PTC, (red): PC-PTC1, and (blue): PC-PTC2.

Fig. 6 shows the results of both criteria over a stator frequency $3\text{Hz} \leq f \leq 36\text{Hz}$, which corresponds to a rotor speed $5\text{rad/s} \leq \Omega_r \leq 105\text{rad/s}$ under a constant load torque T_l = 1N.m. From Fig. 6(1), it can be noted that the C-PTC method is penalized by high switching frequencies at low speed operation, while the proposed PC-PTC1 and PC-PTC2 methods mitigate the values of f_{sw} for $f < 20$Hz (i.e $\Omega_r < 60$rad/s). Nevertheless, the C-PTC method exhibits slight reduction of f_{sw} at high speed range. Indeed, as previously noted in the simulation results of Fig. 5 and confirmed by the results of Fig. 6(1), the 120◦-phase-clamping, which is self-applied by the C-PTC method at high speeds, leads to further reduction of the switching frequency compared to the PC-PTC methods, which are based on the 60°-phase-clamping technique.

Concerning the current THDs shown in Fig. 6(2), one can notice that the PC-PTC1 method exhibits the lowest harmonic distortion over the speed range. On the contrary, the proposed PC-PTC2 method, compared to the C-PTC, mitigates the THD values only at low speeds. The quantitative comparison proves the superiority of the proposed PC-PTC methods over the C-PTC in terms of reduction of switching frequency and current harmonic distortion at low speeds below $|\Omega_r| <$ 40% of rated speed.

Experimental Results

The experimental study has been carried out in an attempt to highlight the improvements gained by the proposed PC-PTC methods with respect to the C-PTC. The three PTC methods are implemented on a test setup of a B6 inverter fed IM drive platform, which is illustrated in Fig. 7. A dSPACE 1104 digital controller is employed to achieve the control algorithms. The selected experimental results are acquired via digital/analog converters of the connector panel except the voltages and currents, which are measured by voltage and current sensors. All experimental data are recorded on a digital oscilloscope. The rotor speed is measured through a 1024 pulse/rotation encoder coupled to the IM shaft.

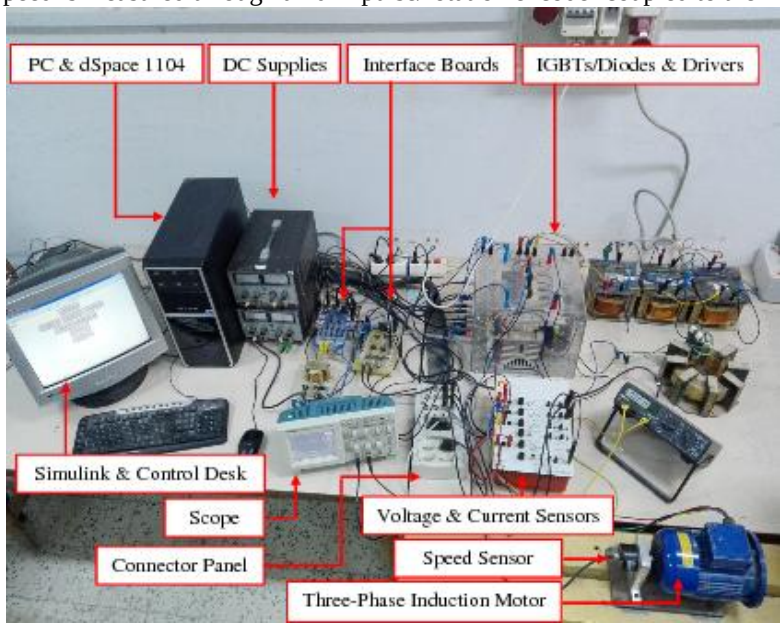

Fig. 7 Photograph of the experiment setup used to evaluate the performance of the three PTC strategies

Figs. 8 to 10 present the steady-state experimental results of the C-PTC (subscript a), PC-PTC1 (subscript b), and PC-PTC2 (subscript c) methods, considering low and high rotor speeds, such as: Ω_r = 30rad/s (subscript 1), and Ω_r = 120rad/s (subscript 2).

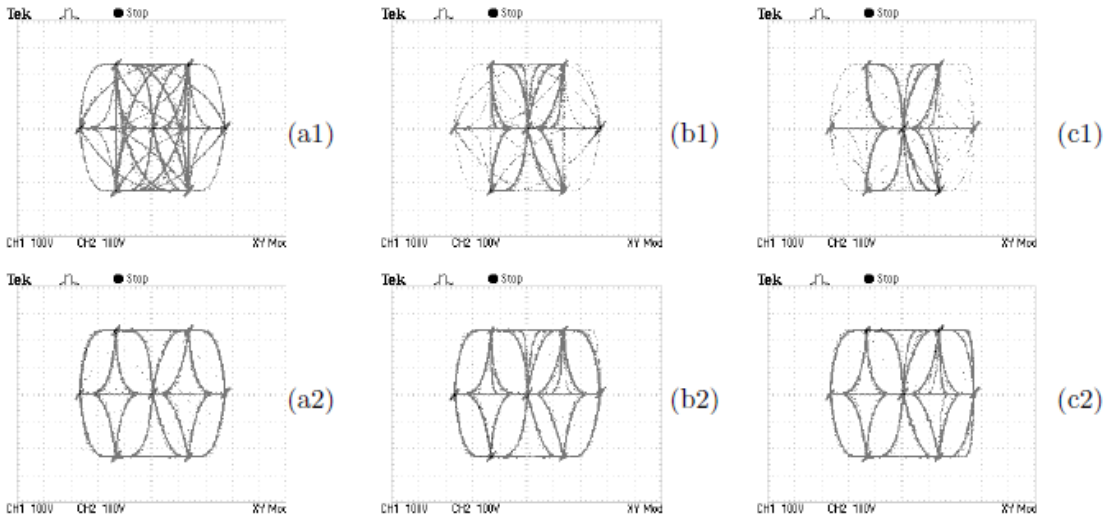

Fig. 8 Steady-state experimental results of the locus described, in the stationary $\alpha\beta$-plane, by the extremity of the voltage vector V_s (100V/div). Legend 1 (1): case of Ω_r = 30rad/s and (2): case of Ω_r = 120rad/s. Legend 2 (a): C-PTC, (b): PC-PTC1, and (c): PC-PTC2.

Fig. 8 shows the locus described by the extremity of the voltage vector $\mathbf{V}_s$ in the stationary $\alpha\beta$-plane. These shapes clearly highlight the summits of the voltage vectors $\mathbf{V}_i$ and the commutations between these vectors. At low speed operation, it is clearly seen from Fig. 8(a1) that the commutations between the opposite voltage vectors ($\mathbf{V}_2 \longleftrightarrow \mathbf{V}_5$) and ($\mathbf{V}_3 \longleftrightarrow \mathbf{V}_6$) are frequently occurring under the C-PTC method. It is to be noted that these commutations change the states of the six power switches of the B6 inverter.

On the contrary and as shown in Figs. 8(b1) and 8(c1), the phase-clamping techniques minimize the transitions between the opposite vectors. In fact, these transitions are limited while moving from sector to another, as indicated in Tables-1 to

4. Hence, the proposed PC-PTC methods mitigate the switching power losses at low speeds compared to the C-PTC strategy. In the case of high speed, the locus described by $\mathbf{V_s}$ under the three PTC methods are almost similar, as illustrated in Figs. 8(a2)-(c2). These remarks confirm the simulation results corresponding to the switching frequency f_{sw} of Fig. 6(1).

Fig. 9 presents the waveforms of the stator a-phase voltage v_{an} and current i_{as}. It can be observed that, at low speed, the waveforms of v_{an} present low harmonic distortion in the case of the PC-PTC1 and PC-PTC2 methods. However, it can be remarked that, at high speed, the voltage and current waveforms yielded by the three PTC strategies are almost similar, as shown in Figs. 9(a2)-(c2). As noted in the simulation-based current THDs (see Fig. 6(2)), these experimental results prove that the phase-clamping technique reduces the harmonic distortion of the stator voltages and currents at low speed operation.

In order to confirm that the two proposed PC-PTC methods attenuate the torque ripple compared to that yielded by the C-PTC strategy, Fig. 10 shows the experimental results of the sector successions with the electromagnetic torque waveforms. It can be seen that the PC-PTC1 and PC-PTC2 strategies are found to be significantly better than the C-PTC method in terms of torque ripple reduction at low speeds. For instance and referring to Figs. 10(a1)-(c1), the torque ripple ΔT_{em} yielded by the C-PTC, PC-PTC1, and PC-PTC2 methods are equal to 2.05N.m, 1.2N.m, and 1.15N.m, respectively, which means that the proposed PC-PTC reduce by 40% of the torque ripple yielded by C-PTC. On the other hand, it is clear that the increase of the motor speed leads to comparable torque ripple for the three PTC methods.

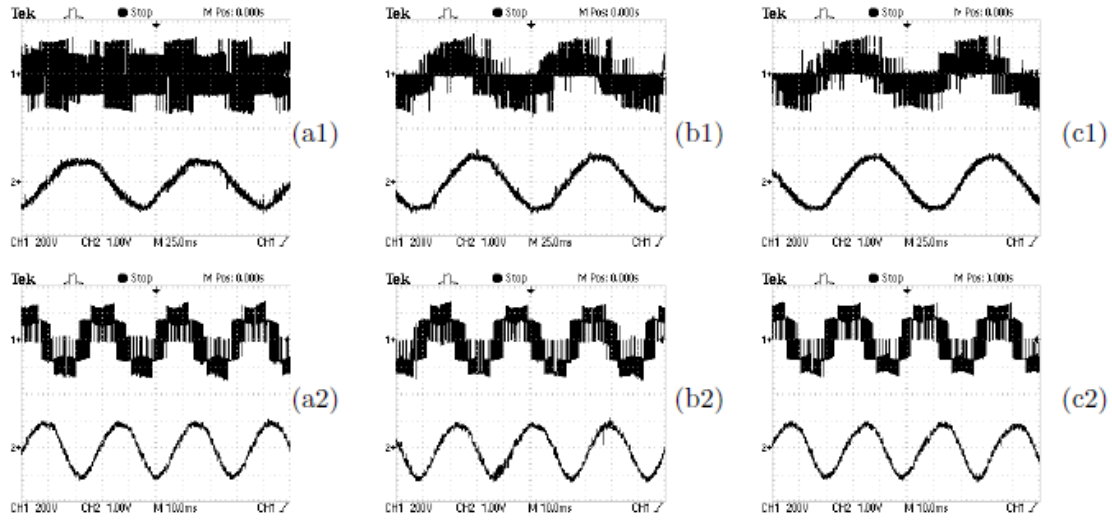

Fig. 9 Steady-state experimental results of the stator a-phase voltage v_{an} (200V/div) and current i_{as} (1A/div). Legend 1 (1): case of Ω_r = 30rad/s and (2): case of Ω_r = 120rad/s. Legend 2: (a): C-PTC, (b): PC-PTC1, and (c): PC-PTC2.

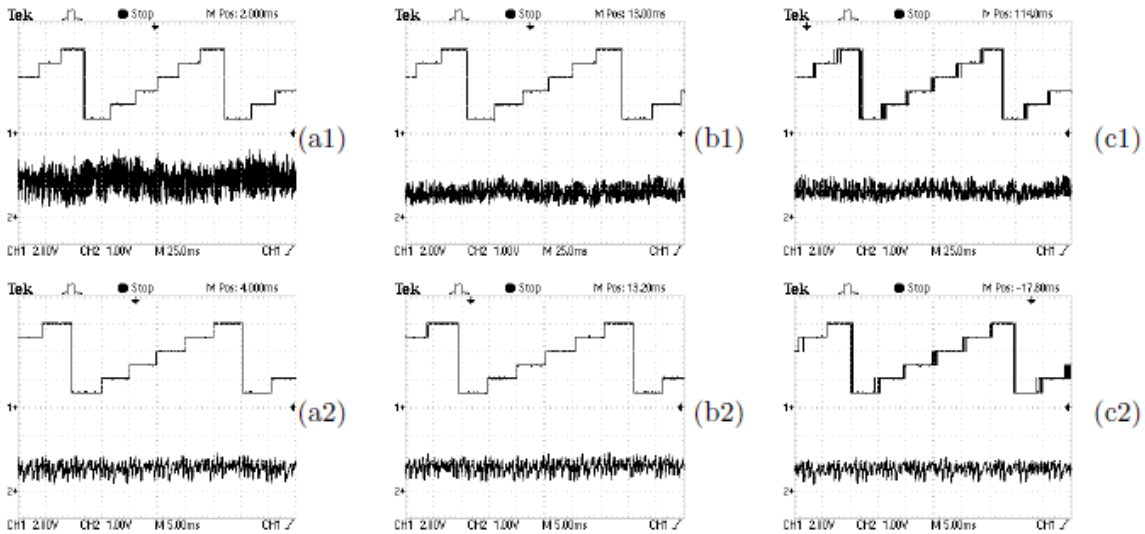

Fig. 10 Steady-state experimental results of the sector successions (2 sectors/div) with the electromagnetic torque waveforms (0.5N.m/div). Legend 1 (1): case of Ω_r = 30rad/s and (2): case of Ω_r = 120rad/s Legend 2 (a): C-PTC, (b): PC-PTC1, and (c): PC-PTC2.

CONCLUSION

This paper has been focused on the synthesis and performance analysis of three PTC methods dedicated to control the B6 inverter fed IM drives. In addition to the conventional PTC (C-PTC) strategy, two novel PTC methods based on the well-known phase-clamping (PC) techniques have been proposed. In an attempt to reduce the switching frequency, current harmonic distortion and torque ripple, the developed PC-PTC methods have been founded on the basis of modulating two inverter legs instead of the three ones by clamping, during each 60° sub-cycle, one stator phase to the positive or negative terminals of the dc-bus voltage. Nevertheless, in the developed PC-PTC methods only four voltage vectors (one zero and three active vectors) have been evaluated for the prediction, optimization, and actuation, during each one-sixth of the stator period.

The difference between the PC-PTC1 and PC-PTC2 methods is the approach adopted in the selection of the clamped phase, where the revolving reference vector is the stator flux vector $\boldsymbol{\psi}_s$ and the stator current vector $\mathbf{I}_s$ in the case of PC-PTC1 and PC-PTC2, respectively. The performance of the developed PC-PTC methods have been evaluated through simulation and experimental results considering various criteria, such as: voltage vectors transitions, stator current THD, switching frequency, and torque ripple. It has been shown that, at low speed operation, the proposed PC-PTC methods exhibit high performances in terms of reduction of switching frequency, stator current THD, and torque ripple compared to the C-PTC strategy. Furthermore, the three PTC methods are characterized by similar performances for the case of high speed operation.

REFERENCES

[1]. Y. Zhang, H. Yang, and B. Xia, "Model-predictive control of induction motor drives: torque control versus flux control," *IEEE Trans. Ind. Appl.*, vol. 52, no. 5, pp. 4050-4060, Sep./Oct. 2016.

[2]. Z. Zhou, C. Xia, Y. Yan, Z. Wang, and T. Shi, "Torque ripple minimization of predictive torque control for PMSM with extended control set," *IEEE Trans. Ind. Electron.* vol. 64, no. 9, pp. 6930-6939, Sep. 2017.

[3]. Md. Habibullah, D. D. C. Lu, D. Xiao, J. E. Fletcher, and M. F. Rahman, "Low complexity predictive torque control strategies for a three-level inverter driven induction motor," *IET Electr. Power Appl.*, vol. 11, no. 5, pp. 776-783, May 2017.

[4]. Y. Cho, Y. Bak, and K. B. Lee, "Torque-ripple reduction and fast torque response strategy for predictive torque control of induction motors," *IEEE Trans. Power Electron.*, vol. 33, no. 3, pp. 2458-2470, Mar. 2018.

[5]. W. Xie, X. Wang, F. Wang, W. Xu, R. M. Kennel, D. Gerling, and R. D. Lorenz, "Finite-controlset model predictive torque control with a deadbeat solution for PMSM drives," *IEEE Trans. Ind. Electron.*, vol. 62, no. 9, pp. 5402-5410, Sep. 2015.

[6]. W. Xie, X. Wang, F. Wang, W. Xu, R. Kennel, and D. Gerling, "Dynamic loss minimization of finite control set-model predictive torque control for electric drive system," *IEEE Trans. Power Electron.*, vol. 31, no. 1, pp. 849-860, Jan. 2016.

[7]. Md. Habibullah, D. D. C. Lu, D. Xiao, and M. F. Rahman, "A simplified finite-state predictive direct torque control for induction motor drive," *IEEE Trans. Ind. Electron.*, vol. 63, no. 6, pp. 3964-3975, Jun. 2016.

[8]. Y. Zhang and H. Yang, "Model predictive torque control of induction motor drives with optimal duty cycle control," *IEEE Trans. Power Electron.*, vol. 29, no. 12, pp. 6593-6603, Dec. 2014.

[9]. Y. Zhang and H. Yang, "Generalized two-vector-based model-predictive torque control of induction motor drives," *IEEE Trans. Power Electron.*, vol. 30, no. 7, pp. 3818-3829, Jul. 2015.

[10]. X. Zhang and B. Hou, "Double vectors model predictive torque control without weighting factor based on voltage tracking error," *IEEE Trans. Power Electron.*, vol. 33, no. 3, pp. 2368-2380, Mar. 2018.

[11]. S. Das, A. C. Binojkumar, and G. Narayanan, "Analytical evaluation of harmonic distortion factor corresponding to generalised advanced bus-clamping pulse width modulation," *IET Power Electron.*, vol. 7, no. 12, pp. 3072-3082, Jul. 2014.

[12]. A. C. Binojkumar, B. Saritha, and G. Narayanan, "Experimental comparison of conventional and bus-clamping PWM methods based on electrical and acoustic noise spectra of induction motor drives," *IEEE Trans. Ind. Appl.*, vol. 52, no. 5, pp. 4061-4073, Sep./Oct. 2016.

[13]. V. S. S. P. K. Hari and G. Narayanan, "Theoretical and experimental evaluation of pulsating torque produced by induction motor drives controlled with advanced bus-clamping pulse width modulation," *IEEE Trans. Ind. Electron.*, vol. 63, no. 3, pp. 1404-1413, Mar. 2016.

[14]. B. El Badsi, B. Bouzidi, and A. Masmoudi, "Bus-clamping-based DTC: an attempt to reduce harmonic distortion and switching losses," *IEEE Trans. Ind. Electron.*, vol. 60, no. 3, pp. 873-884, Jun. 2013.

[15]. A. Ouarda, B. El Badsi, and A. Masmoudi, "Bus-clamping-based direct torque control strategy dedicated to B6 inverter fed symmetrical two-phase IM drive," *IEEE Trans. Ind. Electron.*, vol. 65, no. 7, pp. 5344-5352, Jul. 2018.

[16]. W. Zouari and B. El Badsi, "Comparative investigation of bus-clamping PTC strategies for IM drives," in *Proc. IEEE 12th Int. Conf. Ecological Vehicles and Renewable Energies (EVER)*, Monte Carlo, Monaco, Apr. 2017.

[17]. Y. Zhang, W. Xie, Z. Li, and Y. Zhang, "Low-complexity model predictive power control: Double-vector-based approach," *IEEE Trans. Ind. Electron.*, vol. 61, no. 11, pp. 5871-5880, Nov. 2014.

[18]. Y. Zhang, H. Yang, and B. Xia, "Model predictive torque control of induction motor drives with reduced torque ripple," *IET Electr. Power Appl.*, vol. 9, no. 9, pp. 595-604, Sep. 2015.
[19]. Y. Zhang and H. Yang, "Two-vector-based model predictive torque control without weighting factors for induction motor drives," *IEEE Trans. Power Electron.*, vol. 31, no. 2, pp. 1381-1390, Feb. 2016.
[20]. S. A. Davari, D. A. Khaburi, and R. Kennel, "An improved FCS-MPC algorithm for an induction motor with an imposed optimized weighting factor," *IEEE Trans. Power Electron.*, vol. 27, no. 3, pp. 1540-1551, Mar. 2012.
[21]. F. Villarroel, J. R. Espinoza, C. A. Rojas, J. Rodriguez, M. Rivera, and D. Sbarbaro, "Multiobjective switching state selector for finite-states model predictive control based on fuzzy decision making in a matrix converter," *IEEE Trans. Ind. Electron.*, vol. 60, no. 2, pp. 589-599, Feb. 2013.
[22]. C. A. Rojas, J. Rodriguez, F. Villarroel, J. R. Espinoza, C. A. Silva, and M. Trincado, "Predictive torque and flux control without weighting factors," *IEEE Trans. Ind. Electron.*, vol. 60, no. 2, pp. 681-690, Feb. 2013.
[23]. P. Cortes, M. P. Kazmierkowski, R. M. Kennel, D. E. Quevedo, and J. Rodriguez, "Predictive control in power electronics and drives," *IEEE Trans. Ind. Electron.*, vol. 55, no. 12, pp. 4312- 4324, Dec. 2008.